MICROCOPY RESOLUTION TEST CHART

NATIONAL BUREAU OF STANDARDS-1963-A

OFFICE OF NAVAL RESEARCH

N00014-80-K-0852

Task No. 056-681

Technical Report No. 10
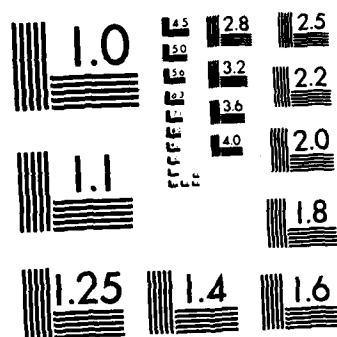
COMPARISON OF PHOTON STIMULATED DISSOCIATION

OF GAS PHASE, ~~CONDENSED~~, AND CHEMISORBED WATER
SOLID

By

David E. Ramaker

Prepared for Publication

in

Chemical Physics

DTIC
ELECTE
S NOV 2 3 1983
D
B

George Washington University
Department of Chemistry
Washington, D.C. 20052

September 1983

Reproduction in whole or in part is permitted for any purpose
of the United States Government

This document has been approved for public release and sale;
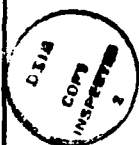its distribution is unlimited

AD-A134 986

DTIC FILE COPY

REPORT DOCUMENTATION PAGE	READ INSTRUCTIONS BEFORE COMPLETING FORM

1. REPORT NUMBER No. 10	2. GOVT ACCESSION NO. A134986	3. RECIPIENT'S CATALOG NUMBER

4. TITLE (and Subtitle) COMPARISON OF PHOTON STIMULATED DISSOCIATION OF GAS PHASE, ~~CONDENSED~~ SOLID, AND CHEMISORBED WATER.	5. TYPE OF REPORT & PERIOD COVERED Technical Report
	6. PERFORMING ORG. REPORT NUMBER

7. AUTHOR(s) David E. Ramaker	8. CONTRACT OR GRANT NUMBER(s) N00014-80-K-0852

9. PERFORMING ORGANIZATION NAME AND ADDRESS Chemistry Department George Washington University Washington, D.C. 20052	10. PROGRAM ELEMENT, PROJECT, TASK AREA & WORK UNIT NUMBERS Prog. Elem. No. 61153N Task Area No. PP.013-08-01 Work Unit # NR 056-681

11. CONTROLLING OFFICE NAME AND ADDRESS Office of Naval Research, Dept. of Navy 800 N. Quincy Street Washington, D.C. 22217	12. REPORT DATE Sept. 83
	13. NUMBER OF PAGES 24

14. MONITORING AGENCY NAME & ADDRESS(if different from Controlling Office)	15. SECURITY CLASS. (of this report) Unclassified
	15a. DECLASSIFICATION/DOWNGRADING SCHEDULE

16. DISTRIBUTION STATEMENT (of this Report)

This document has been approved for public release and sale; its distribution is unlimited.

17. DISTRIBUTION STATEMENT (of the abstract entered in Block 20, if different from Report)

19. KEY WORDS (Continue on reverse side if necessary and identify by block number)

Photon stimulated desorption, photo-dissociation, fragmentation, electron stimulated desorption, Water.

20. ABSTRACT (Continue on reverse side if necessary and identify by block number)

Recent electron-and-photon-stimulated desorption (ESD/PSD) data for H_2O in the condensed phase and chemisorbed on GaAs(110) and Ti(001) are interpreted utilizing previously published photoelectron, electron coincidence and Auger data along with theoretical calculations. Comparison with fragmentation data from the gas phase indicates that only two hole-one electron type states are effective for desorption in condensed or molecularly chemisorbed hydrogen bonded water. The $1b_2^{-1}$ excitation, which effectively dissociates H_2O gas via predissociation, is

ineffective in the condensed phase because of the presence of intermolecular decay mechanisms which compete with the predissociation process. Hydrogen bonding reduces the effectiveness of the " $2a_2^{-1}$ " excitation for H^+ desorption. The $1b_1^{-1} 3a_1^{-1} 4a_1$ two hole-one electron states are sufficiently long lived; occupation of the strongly antibonding $4a_1$ orbital also makes them repulsive. These properties make the two hole-one electron states the most persistent for H^+ desorption from the H_2O phase studied. The core level PSD spectrum from solid D_2O is also interpreted. All of the results are found to be comparable to previously reported results for CO.

Accession For

NTIS GRA&I

DTIC TAB

Unannounced

Justific

PER CALL JC

By

Distribution/

Availability Codes

Avail and/or

Dist | Special

A-1

COMPARISON OF PHOTON-STIMULATED DISSOCIATION OF GAS-PHASE, SOLID AND CHEMISORBED WATER

David E. RAMAKER *

Surface Science Division, National Bureau of Standards, Washington, DC 20234, USA
and *Chemistry Department** , George Washington University, Washington, DC 20052, USA*

Recent electron- and photon-stimulated desorption (ESD/PSD) data for H_2O in the condensed phase and chemisorbed on GaAs(110) and Ti(001) are interpreted utilizing previously published photoemission, electron coincidence and Auger data along with theoretical calculations. Comparison with fragmentation data from the gas phase indicates that only two hole–one electron type states are effective for desorption in condensed or molecularly chemisorbed hydrogen bonded water. The $1b_2^{-1}$ excitation, which effectively dissociates H_2O gas via predissociation, is ineffective in the condensed phase because of the presence of intermolecular decay mechanisms which compete with the predissociation process. Hydrogen bonding reduces the effectiveness of the "$2a_1^{-1}$" excitation for H^- desorption. The $1b_2^{-2}4a_1$ and $1b_2^{-1}3a_1^{-1}4a_1$ two hole–one electron states are sufficiently long lived; occupation of the strongly antibonding $4a_1$ orbital also makes them repulsive. These properties make the two hole–one electron states the most persistent for H^- desorption from the H_2O phases studied. The core level PSD spectrum from solid D_2O is also interpreted. All of the results are found to be comparable to previously reported results for CO.

1. Introduction

Recent comparative investigations of dissociation processes in gas phase, condensed (solid) and chemisorbed CO [i.e. CO(g), CO(s) and CO/Ru(001) or CO/Ni(100)] revealed several mechanisms are responsible for dissociation of CO [1]. Major differences in the ion yield spectra were also revealed. These differences were attributed to adsorbate–substrate and adsorbate–adsorbate interactions providing for additional alternative decay mechanisms of the excited states which initiate the dissociation or desorption [2]. Identification of the excited states responsible for dissociation indicates they possess widely different electronic character and hence arise from widely different excitation mechanisms [3]. To further understand these mechanisms, and the role of covalent interactions on these mechanisms, further investigations are needed.

In this work, details of a similar comparative investigation of dissociation processes in gas phase, condensed and chemisorbed H_2O are reported. This investigation is made possible by recent reports of PSD data for $H_2O(s)$ [4,5], $H_2O/$ GaAs(110) [6], and $H_2O/Ti(001)$ [7]. Recent photodissociation data [8,9], electron–electron and electron–ion coincidence data [(e, 2e) and (e, e + ion)] [10], and theoretical interpretations of photoemission data for $H_2O(g)$ [11] also make this detailed comparison possible at this time. Results of this comparison are given in section 3 and discussed in section 4. Comparison of the results with those found for CO, and conclusions from these investigations, are given in section 5. To assist in the PSD data analysis, a detailed investigation of the valence-orbital structure in the H_2O systems involved is presented in section 2.

A general review of electron- and photon-stimulated desorption processes in molecular and ionic systems, and for chemisorbed systems, has recently been published [12]. In covalent systems, at least three mechanisms have been identified
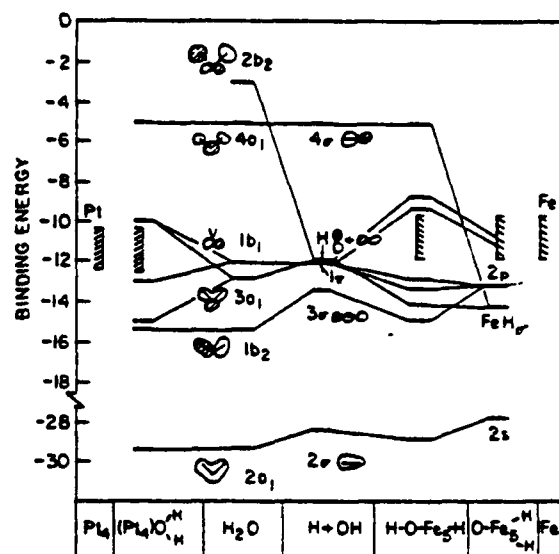
[12]. In covalent systems, at least three mecha-
nisms have been identified [3]. They can be cate-
gorized by the character of the excitation initiating
the desorption or dissociation. A one-electron
Franck–Condon excitation resulting in a one-hole
or one hole–one electron excited state (1h or 1h1e
state) initiates desorption if the excited state is
sufficiently repulsive and long lived. This is known
as the Menzel–Gomer–Redhead model [13]. In
ionic systems, the Knotek–Feibelman model indi-
cates a core-hole Auger decay creates a two hole
(2h) state which initiates desorption via the rever-
sal of the Madelung potential [14]. In extended
covalent systems, the 2h state is sufficiently long
lived only if the effective hole–hole repulsion, U^e,
is greater than the corresponding covalent interac-
tion, V (i.e. $U^e > V$) [15]. In isolated small mole-
cules, the 2h state frequently initiates a Coulomb
explosion [16]. Finally, two hole–one electron
(2h1e) states may also initiate desorption or dis-
sociation [1]. Within the sudden approximation
and configuration interaction (CI) theory [11,1]
these states derive their excitation probability by
configuration mixing with 1h ionic states nearly
degenerate in energy. For CO/Ru, the 2h1e states
are the most important for O^+ and CO^+ desorp-
tion [1]. In this work, the dissociation processes in
the various H_2O phases studied will be examined
with a view toward identifying the specific ionic
states initiating the dissociation, and hence toward
determining which models are active in each phase.

2. H_2O valence electronic structure

2.1. Occupied orbitals

The valence electronic structure pof $H_2O(g)$ has
been well studied both theoretically and experi-
mentally. The one-electron orbitals, labeled
according to C_{2v} symmetry, are schematically indi-
cated in fig. 1. Orbital energies can be determined
from the X-ray and ultraviolet photoemission (XPS
and UPS) data in fig. 2 [17–20]. In the deep
valence region, the $2a_1$ orbital is largely of O(2s)
parentage (74%), and consequently is often char-
acterized as a "core" orbital [17]. However, energy
considerations reveal the $2a_1$ orbital contributes

Fig. 1. Results of semi-emperical LCAO MO calculations sum-
marizing the molecular-orbital energy levels for the various
H_2O structures indicated [29]. MO binding energies are given
relative to the vacuum. The H_2O orbitals are indicated sche-
matically and labeled in the C_{2v} point group. The $4a_1$ and $2b_2$
orbital energies are obtained from experiment [49].

about 20% to the total H–O bond energy [20]. The
$1b_2$ orbital contributes most of the remaining bond
energy and is characterized as a bonding orbital.
The $3a_1$ and $1b_1$ orbitals may be characterized as
oxygen lone-pair orbitals. Unoccupied or virtual
orbitals include a weakly antibonding $2b_2$ orbital
and strongly antibonding $4a_1$ orbital.

The valence electronic structure of condensed
or solid H_2O (ice) has also been well characterized
[17,18,21–25]. Recently, the many experimental
and theoretical papers have been analyzed and
condensed to give the overview presented in fig. 3.
Hexagonal ice is obtained for temperatures above
173 K; below 153 K cubic ice is formed. Con-
densation of water vapor kept below 123 K leads
to amorphous ice [23]. The effect of these different
crystalline forms on the XPS, UPS and UV
absorption spectra appears to be nearly negligible,
indeed even the differences between $H_2O(g)$ and
$H_2O(s)$ are relatively small. Small shifts in the
ionization potentials (IP(gas) – IP(solid) $\approx$ 1 eV)
have been indicated [18]. These have been attri-
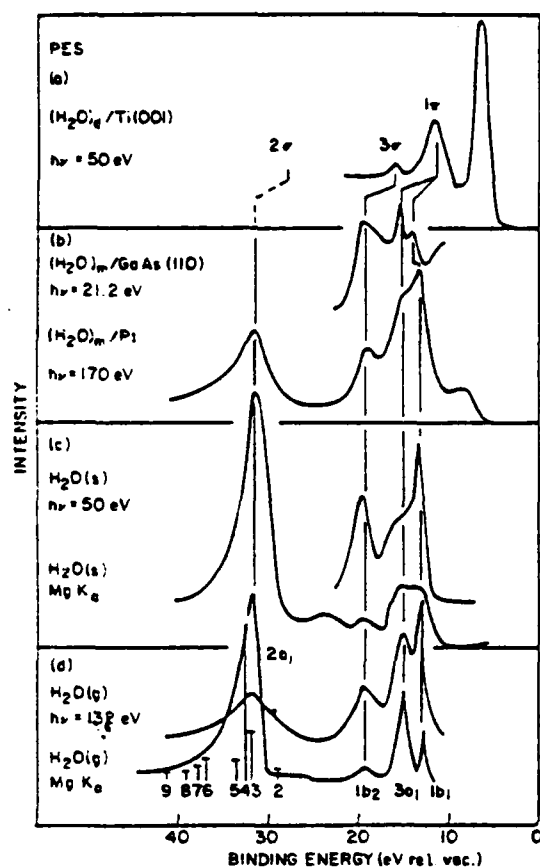buted largely to relaxation or polarization energy

Fig. 2. Comparison of photoemission spectra from $(H_2O)_a/Ti$ [7], $(H_2O)_m/GaAs$ [40], $(H_2O)_m/Pt$ [28], $H_2O(s)$ at $h\nu = 50$ eV [7] and MgKα [17] and $H_2O(g)$ at $h\nu = 132$ eV [20] and MgKα [17]. The binding-energy scale is relative to the vacuum for $H_2O(g)$; the remaining spectra (except for OH/Ti) have been shifted slightly for alignment of the $1b_2$ peak. The lines under the $2a_1$ peak in part (d) indicate the intensities of the various satellite contributions as determined from the Cl calculations of Arneberg et al. [11]. The numbers on these lines correspond to those in table 1, not those in ref. [11].
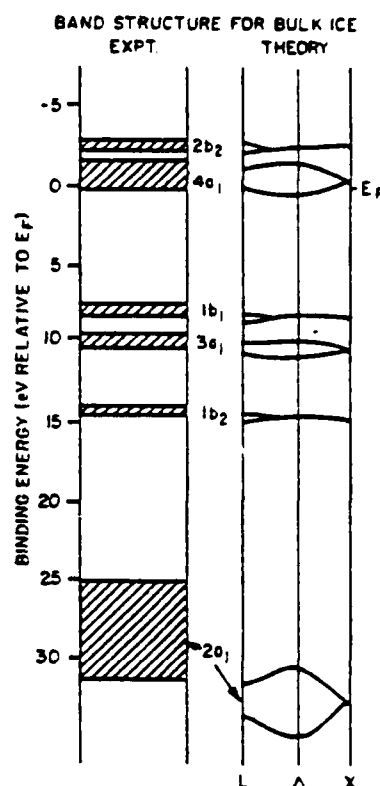

Fig. 3. *Experiment.* Electron energy levels of bulk ice as deduced by Rosenberg et al [4], from experiments reported in the literature. *Theory.* Results from the band-structure calculations of Parravicini and Resca [24] and reported in ref. [4].

differences between the vapor and ice phases, since hydrogen bonding is expected to shift some of the levels in the opposite direction [18]. The most important difference between the vapor and ice spectra evident in fig. 2 is the large broadening of the $3a_1$ orbital due to hydrogen bonding. The large width of the $2a_1$ peak in both the gas- and solid-phase spectra of fig. 2 reflects the Franck–Condon envelope and the addition of satellites also of large width to this peak. Fig. 3 indicates however that

all three of the a_1 bands are broadened in $H_2O(s)$ from hydrogen bonding.

The large broadening of the a_1 orbitals, and apparent lack of similar broadening of the b_1 and b_2 orbitals, is of general interest, but it is paramount to an understanding of the PSD H^- yield to be discussed in section 3. Ab initio calculations on H_2O dimers indicate the a_1 orbitals facilitate electron motion "longitudinal" or parallel to the O–O or H bond axis, where as the non-a_1 orbitals allow electron motion only in a direction perpendicular or "transverse" to the H-bond axis [26,27]. In the context of MO theory, the matrix elements coupling pairs of a_1 orbitals are larger than for pairs of non-a_1 orbitals. Thus even in linear H_2O dimers, the bonding and antibonding a_1-orbital combinations show a large energy

separation (2-5 eV) [27]. In band calculations [24], this broadening is referred to as "Davydov splitting" from interaction between two molecules of different orientation in the unit cell, but its source is the same.

The chemisorption of H_2O on many metals has ~~metals~~ has little effect on the H_2O UPS spectrum [28]. indeed the differences in the UPS peak energies between H_2O/Pt and $H_2O(g)$ are less than between $H_2O(s)$ and $H_2O(g)$ (fig. 2). This indicates along with other data [29–39] that the water is molecularly chemisorbed, the bonding to the surface occurring through the oxygen atom. Semiempirical LCAO MO calculations indicate the bonding occurs through the O lone-pair orbitals (fig. 1) [29,30]. The theoretical results in fig. 1 predict a larger shift than the UPS spectrum indicates however. The broadening of the a_1 UPS bands for H_2O/Pt indicates hydrogen bonding also occurs on the surface. Recent studies for H_2O on Ru(001) [31,32]; W(100), Pt(100) [33], Pt(111) [34]. Cu(100) [35] and Rh(111) [36] all indicate molecular chemisorption to the metal through the O atom, but with island formation also occurring as a result of hydrogen bonding.

Specific models for the structure of H_2O clusters adsorbed in vacuum on metal surfaces, as well as for bulk ice, have been proposed; some are more convincing than others. Comprehensive studies of $H_2O/Ru(001)$ utilizing UPS, electron-stimulated desorption ion angular distributions (ESDIAD), low-energy electron diffraction (LEED), thermal desorption mass spectroscopy (TDMS), electron energy loss spectroscopy (EELS), angle resolved EELS, and Auger electron spectroscopy (AES) reveal the formation of a bilayer of hydrogen bonded H_2O [37,38]. The model consistent with the data indicates the first layer consists of H_2O molecules bonded to the surface via the O atom, with H atoms pointed symmetrically away from the surface. The second layer has each O atom hydrogen bonded to a hydrogen atom in the first layer, and one H atom of each H_2O in the second layer H-bonded to an O atom in the first layer. This leaves the remaining H atom pointed outward almost perpendicular to the surface [37,38]. A rather different structure has been proposed for $H_2O/Pt(100)$, namely a cyclohexane-like

structure with many of the first layer molecules hydrogen bonded to the Pt surface [33]. At low coverage, most of the H_2O in the hexamer form Pt-O bonds, but these bonds break as the coverage increases. These structures can be compared to the surface structure of ice. In amorphous ice, six types of sites are distributed over the surface, three with the hydrogens pointed out, three with the hydrogens in [4]. However, the hydrogen out sites seem to be thermodynamically favored, and in any event the ESD active sites are apparently only those with the H atoms pointed out [4,31]. In epitaxially grown ice multilayers, a similar surface structure has been proposed (i.e. half of the molecules have the H atoms pointed outward) [37]. How dependent the ESD/PSD H^+-ion yields (i.e. the desorption mechanism) might be on the surface structure is not yet clear. An important conclusion of this work is that the ion yields are at least dependent on the existence of hydrogen bonding on the surface, and hence probably also on the structure. The ion angular distributions (ESDIAD) are known to be dependent on surface structure, this technique has been used to study the surface structure of H_2O on clean Ni(111) [39] and Ru(001) [31,38], and for H_2O coadsorbed with O on Ni(111) [39] and Ru(001) [38].

UPS data for H_2O chemisorbed on a semiconductor such as GaAs(110) [40] (fig. 2) indicate the H_2O is molecularly chemisorbed through the O atom also in this case. The bonding through the lone-pair orbitals is clearly indicated in this system by the negative shift of the $1b_1$ UPS peak by ≈ 1.0 eV. On other semiconductor surfaces such as Si(100) and Si(111), the UPS data suggest that at room temperature H_2O molecularly chemisorbs here also; however, EELS data clearly indicate that H_2O dissociates to give Si-H and Si-OH bonds at this temperature [41]. This difference between the Si and GaAs system suggests a comparison of the H^+ PSD spectra would be most revealing. unfortunately the author is not aware of any PSD data for H_2O/Si in this spectral range.

In contrast to the metals and semiconductors discussed above, H_2O dissociates to form H(ads) and OH(ads) on Ti(001) even at 90 K [7]. This is evident from the very different UPS spectrum shown in fig. 2. The $1b_1$ and $3a_1$ H_2O orbitals are

now merged into a 1π OH orbital and all of the valence orbitals are shifted up in energy. This energy shift is believed to arise from a relaxation energy difference; i.e., the OH–M interaction is much stronger than the H_2O–M interaction. Some intensity under the "1π" peak at 10 eV bonding energy is believed to originate from atomic oxygen on the surface (i.e. coming from completely dissociated H_2O), but this is not expected to appreciably alter the PSD H^+ ion yield. The presence of O, OH and H on the surface indicates the H_2O exposed surface might best be referred to as $(H_2O)_d$/Ti (where 'd' refers to dissociated) rather than OH/Ti. This $(H_2O)_d$/Ti notation is used throughout this paper. For molecularly chemisorbed systems, $(H_2O)_m$ is used (where m refers to molecular).

Fig. 1 shows the results of theoretical calculations for OH + H on Fe(100), where the H_2O is also known to dissociatively chemisorb [42]. These calculations indicate Fe is more reactive than Pt toward H_2O because the Fe orbitals are more

diffuse, and because the Fe s–d band lies further away from the H_2O energy levels causing the H_2O–Fe antibonding orbitals to be emptied [29]. This is also expected to be true for Ti. The small-cluster calculations of fig. 1 do not show the larger relaxation energy which decreases the binding energy of the 1π and 3σ orbitals. Finally, note that the $2b_2$ orbital becomes the Fe–H bond orbital which is predicted to be between the 1π and 3σ orbitals [29]. A slight shoulder appears in the UPS spectrum just below the 1π peak, but its source cannot be definitely determined.

In section 1, the importance of the 2h1e states to the dissociation process was briefly discussed. These states may produce satellites in XPS or UPS spectra; they derive their intensity from correlation mixing with 1h states of approximately the same energy [43,46]. In $H_2O(g)$, these satellites introduce a weak structure between 25 and 30 eV binding energy, and also cause an asymmetric lineshape for the $2a_1^{-1}$ peak [11] (fig. 2d). Reported (e, 2e) measurements, which simulates the photo-

Table 1
H_2O UPS satellite results (E_b is the binding energy relative to vacuum; I is the percent intensity of $2a_1^{-1}$ peak)

$^2A_1$ states (dominant configuration)	E_b/I				
	a)	b)	c)	d)	e)
(1) $1b_1^{-1}3a_1^{-1}4a_1$ $\quad\{^4B_1$ $\quad^2B_1$					25.87
(2) $1b_1^{-2}4a_1$	29.11 / 6.8	27.24 / 6.6	27.02 / 0.68		27.59
(3) $3a_1^{-2}4a_1$	32.95 / 26.4	32.29 / 2.5		30.20 / 28.7	
(4) $2a_1^{-1}$	33.48 / 100	31.48 / 100	32.71 / 100	32.4 / 100	34.90
(5) $3a_1^{-1}1b_1^{-1}2b_1$	34.30 / 8.3			33.8 / 2.5	
(6) $3a_1^{-1}1b_2^{-1}2b_2$	37.21 / 20	35.37 / 16	35.18 / 10	37.7 / 14	
(7) $3a_1^{-1}1b_2^{-1}2b_2$	37.85 / 14.7	35.97 / 14	35.39 / 4.1		
(8) $3a_1^{-1}1b_2^{-1}2b_2$	39.75 / 3				
(9) $3a_1^{-1}1b_1^{-1}4b_2$	42.42 / 3.8				

a) Arneberg et al. [11]. SCF CI sudden approximation (1700 ionic configurations); numbers at left refer to fig. 2d.
b) Agren and Siegbahn [45]. SCF CI sudden approximation (62 configurations).
c) Cederbaum [46]. one-particle Greens function.
d) Mishra and Öhrn [48]. 2ph Tamm–Dancoff aproximation.
e) Lecierc et al. [49]. LCAO MO SCF.

emission process. also show the structure around 25–30 eV [44]. In these (e. 2e) data. a clear shoulder appears below the main $2a_1^{-1}$ peak. Fig. 2 indicates the major 2h1e satellites as determined from an SCF CI calculation utilizing 1700 configurations appropriate to the H_2O^- ionic state, and the sudden approximation [11]. The identities of the major numbered satellites are given in table 1 along with the results of other calculations [45–49]. Four other calculations have been indicated in the literature utilizing one-particle Green's functions [46]. the 2ph Tamm–Dancoff [48] approximation, and LCAO MO SCF calculations [49]. as indicated in table 1.

It must be noted that the states are identified by the dominant 2h1e configuration contributing to a many-electron CI-type wavefunction. Within the sudden approximation, the relative intensities are determined by the amount of mixing with the $2a_1^{-1}$ state [11]. The results are basis-set dependent as well as method dependent. In spite of this, the results are reasonably similar for the major satellites.

Most important, from the viewpoint of interpreting the PSD spectra. is the existence of just one major satellite of A_1 symmetry above the "$2a_1^{-1}$" peak. This is probably the source of the satellite structure in the UPS spectrum around 25–30 eV. A satellite of B_1 symmetry (but with an intensity too small to be observed in UPS) is also expected in this region as indicated by the theoretical results of Leclerc et al [49]. The "$2a_1^{-1}$" peak consists of many 2h1e states, the most important being the $3a_1^{-2}4a_1$ state around 32 eV, and several minor ones above 34 eV. Throughout the remainder of this work. all of the states above 32 eV will be referred to collectively as the "$2a_1^{-1}$" spectroscopic state. The $1b_1^{-1}3a_1^{-1}4a_1$, $1b_1^{-2}4a_1$, and "$2a_1^{-1}$" states will be considered further in section 3. The existence of intensity between 25 and 30 eV. and the asymmetry of the "$2a_1^{-1}$" lineshape in the UPS spectrum for $H_2O(s)$ and H_2O/Pt (fig. 2). indicates these same 2h1e satellites exist in these systems.

2.2. Virtual orbitals

Since many of the 2h1e states mentioned above involve the $4a_1$ virtual orbital. and since many of

these 2h1e states will be shown to be important in H_2O dissociation, the character of the $4a_1$ orbital needs to be examined carefully. Outer valence orbital ($1b_2$, $3a_1$, $1b_1$) and K level photoabsorption data [50], partial-channel photoionization data [50,51]. and electron impact data [52,53] (the latter two involving all the valence levels and the O K level) have been reported. The O K level electron-impact spectrum is shown in fig. 4d [53]. These data consistently show an initial broad intense peak (peak 1 in fig. 4d) followed by narrower peaks (peaks 2–4 in fig. 4d). Theoretical calculations attribute this initial peak to excitation into a state with mixed character; i.e. a 3s Rydberg orbital mixed with the $4a_1$ antibonding virtual orbital [49]. Calculations also show an interesting change in the character of this state with the O–H bond length. At small O–H bond lengths this state is largely O(3s)-like, while at large separations it is primarily $4a_1$-like [49,54]. Nevertheless, the large Franck–Condon envelope of peak 1 suggests that. at the equilibrium bond length. this orbital is rather strongly antibonding. Perhaps most convincing of its antibonding character, it is known that the resonant excitations, $1b_1^{-1} \rightarrow (3s, 4a_1)$, $3a_1^{-1} \rightarrow (3s, 4a_1)$ and $1b_2^{-1} (3s, 4a_1)$, all result in dissociation of the H_2O molecule to produce the OH and H radical fragments [50]. This is true even though ionization from the $1b_1^{-1}$ or $3a_1^{-1}$ orbitals does not result in dissociation (to be shown in next section). Thus occupation of the $(3s, 4a_1)$ orbital is critical to the resonant dissociation process, and clearly it is strongly antibonding. Throughout the remainder of this paper. this orbital will simply be referred to as the $4a_1$ orbital, in all the H_2O molecule systems studied

The next higher peak (peak 2) in fig. 4d results from the $1a_1 \rightarrow (np, 2b_2)$ excitation [50,53]. Again the upper state is a mixed orbital, containing both Rydberg and $2b_2$ valence antibonding character [50]. In all three cases where this excitation peak is visible (i.e. from the $3a_1$, $1b_2$, and $1a_1$ initial states), it is much narrower than the $4a_1$ peak. suggesting a smaller virtual-orbital contribution. No evidence for resonant H_2O dissociation into radical fragments is observed from this state. supporting this conclusion [50]. Finally. evidence does exist. both theoretically and experimentally, that the $2b_2$
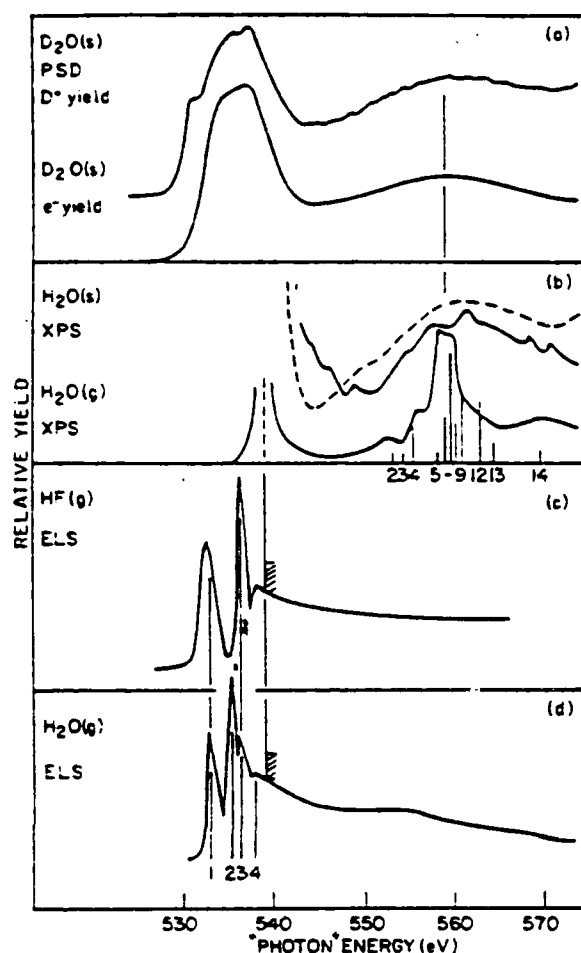
threshold in fig. 4d may be due to this weak mixing.

Peaks 3 and 4 in fig. 4d have been attributed to Rydberg excitations. Peak 3 has been assigned to the $1a_1 \rightarrow 3p$ excitation, peak 4 to the $1a_1 \rightarrow 4s$, p excitations [50,53].

It has already been mentioned in reference to fig. 1, that the $2b_2$ orbital drops out of the H_2O molecule and ends up on the separated hydrogen atom upon dissociation of H_2O to OH and H [29]. This can be seen experimentally by comparing the ELS spectrum of HF(g) [55] in fig. 4c with the $H_2O(g)$ spectrum in fig. 4d. The HF molecule is electronically equivalent to OH^-, and thus it is expected to be similar to OH on the surface of Fe or Ti (e, 2e) [56] and UPS [57] data, and theoretical calculations interpreting the satellite structure for HF [58], all indicate it is similar to OH^-. In any event, the ELS spectrum is not available for the OH radical. In the HF spectrum, the absence of peak 2, which was attributed to the $1a_1 \rightarrow 2b_2$ excitation in H_2O, is striking. The broad weak maximum above the ionization threshold in H_2O is also missing in HF, supporting the suggestion above that the maximum in H_2O arises from $2b_2$ mixing with the continuum. In HF, peak 1 arises from the $1\sigma \rightarrow 4\sigma$ excitation, where the 4σ orbital corresponds to the $4a_1$ in H_2O (see fig. 1).

It seems clear that the $4a_1$ and $2b_2$ virtual antibonding orbitals exist primarily below the ionization thresholds. The partial channel photo-ionization cross sections are consequently free from shape resonances, except for the very weak $2b_2$ resonance mentioned above. This is in marked constrast to the situation in CO where the comparable 6σ antibonding orbital produced large shape resonances in the ionization cross sections. With the 6σ orbital above the ionization threshold, the relatively fast $6\sigma \rightarrow k\sigma$ resonant decay is an important alternative decay mechanism which aborts the dissociation process [1]. This complication yet interesting process cannot occur in H_2O; however, other complicating factors such as hydrogen bonding occur in H_2O which did not enter in CO.

Fig. 4. (a) Comparison of the PSD D^+ yield and total electron yield for solid D_2O as reported in ref. [4]. (b) Comparison of the XPS spectrum for solid (solid line from ref. [46], dashed line from ref. [47]) and gas-phase [11] H_2O. The spectra have been shifted so that the principal peak is in registry with the O K level in $H_2O(g)$ relative to the vacuum as indicated in part d below. The numbered lines correspond to shakeup satellites as determined from the CI calculations of Arneberg et al. [11]. The numbers correspond to those in ref. [11] and those in table 2. (c) The electron loss spectrum for HF gas as reported in ref. [55]. The spectrum has been shifted in energy so that the F K level is in registry with the O K level of $H_2O(g)$ as given in part (d) below. (d) The electron loss spectrum for H_2O gas as reported in ref. [53]. The O K level relative to vacuum is indicated. The numbered loss peaks are discussed in the text.

orbital also mixes with the Kb_2 continuum producing a shape resonance just above the threshold [50]. The broad weak maximum above the

3. Comparison of dissociation and desorption yields

3.1. Core-level excitation

Molecular dissociation as a result of core-level excitation most certainly involves the Auger process. This is true because even the resonant $1a_1^{-1}4a_1$ state (which might be expected to result in dissociation because of occupation of the $4a_1$ antibonding orbital) will undergo a fast (10^{14} s^{-1}) Auger decay before the desorption gets underway. Thus to understand core-level molecular dissociation. one must understand the Auger process.

The O KVV Auger lineshape for $H_2O(g)$ is well known [59]. Several theoretical calculations exist providing a detailed interpretation of the spectrum [60-63]. It is sufficient here to note that just 48% of the total Auger intensity results from n^{-2} hole configurations (i.e. with both holes in the nonbonding orbitals $1b_1^2$ or $3a_1$). The remaining 52% results from one or two holes in a bonding orbital (i.e. $b^{-1}n^{-1}$ or b^{-2}, where b = $1b_2$ or $2a_1$) [61].

The O KVV Auger lineshape for $H_2O(s)$ is very similar to that for $H_2O(g)$, except for an additional large peak at higher energy [64]. This peak has been attributed to a possible splitting off of electron density to higher energies as a result of hydrogen bonding. but the UPS spectrum in fig. 2 does not show such an effect. More likely, this high energy peak results from delocalization of the two holes. It occurs as a consequence of the hydrogen bonding and the broadening of the $3a_1$ band which was indicated in figs. 2 and 3. A rough estimate of the extent of delocalization of the n^{-2} holes can be obtained from the relative magnitudes of the hole–hole repulsion $U_{11} - U_{12}$ in the lone-pair orbitals (the $1b_1$ and $3a_1$), and the lone-pair band width V [65]. U_{11} can be estimated from the $3a_1^2$ Auger peak energy. $E_{K3a_1^2}$ (i.e. $U(3a_1^2) = E_{1a_1} - 2E_{K3a_1^2}$) in $H_2O(g)$, giving a value around 14–15 eV [66,67]. This is consistent with the value used previously for oxygen lone-pair orbitals [65]. U_{12} is around 5 eV as determined previously for O lone-pair orbitals separated by 2.5 Å (the O–O distance in $H_2O(s)$ is 2.75 Å) [65]. V can be estimated from the width of the lone-pair peak in the $H_2O(s)$ UPS spectrum. which is ≈ 4–5 eV. Utilizing calculations reported previously for delocalization of O

lone-pair orbitals. these U_{11}, U_{12}, and V parameters indicate a delocalized contribution of around 10% [65]. It is difficult to estimate quantitatively the amount of delocalized contribution from the Auger lineshape. since the local and delocalized contributions are not completely resolved, but it appears to be significantly larger than 10%. This may arise because of possible intermolecular charge transfer to screen the valence holes in $H_2O(s)$. which effectively reduces U_{11} [68]. This was not included in the above analysis, since U_{11} was obtained from the $H_2O(g)$ spectrum. In any event. it appears that in $H_2O(s)$ the lone-pair holes can delocalize, thereby aborting the Coulomb explosion or dissociation of the H_2O molecule. It is unlikely that $b^{-1}n^{-1}$ or b^{-2} hole configurations undergo much delocalization, since U_{11} is larger in the $2a_1$ orbital and the $1b_2$ bandwidth is very narrow.

Fig. 4a compares the PSD D$^-$ from D$_2$O with the total photoelectron yield (TPY) spectrum [5]. The corresponding data for H_2O are not available but it is assumed the D$_2$O spectra are identical in almost every detail. Before attempting to understand differences between the PSD and TPY spectra, the source of differences between the TPY and the $1a_1$ constant initial state (CIS) photoelectron yield (e.g. similar to fig. 4d) must be understood. The TPY spectrum includes electrons at all energies for particular photon energy, while the $1a_1$ CIS photoelectron yield includes only those electrons with kinetic energy $E_K = h\nu - E_{1a_1}$. Therefore, the TPY spectrum includes not only those electrons from the $1a_1^{-1}$ one-electron excitation but also from shakeup processes (and perhaps also from valence excitation and Auger processes). The XPS spectra for $H_2O(s)$ [46,47] and $H_2O(g)$ [11] in fig. 4b reveal the shakeup features which enter above 550 eV. The principal XPS peak has been aligned with the $1a_1^{-1}$ ionization threshold. It seems clear that the broad maximum which appears in the TPY spectra around 558 eV arises from shakeup, and not from the weak $2b_2$ resonance visible in the $H_2O(g)$ ELS spectrum. Peaks 1 through 4 in the $H_2O(g)$ ELS spectrum merge into one broad peak in the TPY spectrum. This results from broadening of the diffuse virtual orbitals in the solid [5].

Several attempts at interpreting the XPS shakeup spectrum, utilizing a wide variety of theoretical techniques, have been reported in the literature [11,69-72]. Table 2 summarizes these results. Although the results are not in quantitative agreement (for reasons similar to those discussed in reference to table 1), they consistently inidcate two primary shakeup transitions are the $3a_1 \rightarrow 4a_1$ and $1b_2 \rightarrow 2b_2$ transitions. These both involve one of the virtual antibonding valence orbitals. The remaining transitions may be characterized as shakeup from a non-bonding orbital to a Rydberg orbital.

Table 3 gives a summary of the possible initial core excitations, based on the conclusions above. Possible subsequent Auger hole configurations are also indicated. This information is helpful in understanding the differences between the PSD D^+ yield and the TPY spectrum. In table 3, those Auger final states expected to lead to dissociation in $H_2O(s)$ are underlined. These determinations anticipate some conclusions made in the next section, as well as one indicated above. They are: (1) the 1h states n^{-1} and b^{-1} are ineffective for desorption in $H_2O(s)$ because they have insufficient lifetimes; (2) the 2h states $b^{-1}n^{-1}$ and b^{-2}

produce desorption and the n^{-2} states do not for reasons indicated above; (3) all 2h1e states occupying the virtual and strongly antibonding $4a_1$ orbital dissociate; those occupying a Rydberg or the $2b_2$ orbital dissociate only if one of the holes occupies a bonding orbital; and (4) all 3h and 3h1e states dissociate because of the large hole–hole repulsion. Table 3 includes Auger final states in which the shakeup electron acts as a spectator, a participant in the Auger process, or a participant in the shakeoff-Auger process. It is estimated that the relative probability for each process decreases in the order listed. The percent Auger intensity for n^{-2} or $b^{-1}n^{-1} + b^{-2}$ is also given as determined for $H_2O(g)$ [61]. It is assumed this relative intensity does not change appreciably in $H_2O(s)$, and that they hold whether a virtual orbital is occupied or not.

An important result from table 3 is that the $1a_1^{-1}4a_1$, $1a_1^{-1}3a_1^{-1}4a_1$, $1a_1^{-1}1b_2^{-1}2b_2$, and $1a^{-1}n^{-1}R$ core states have a greater probability for eventual H_2O dissociation than do the $1a_1^{-1}R$ or $1a_1^{-1}kl$ states. This conclusion is based on the overall number of underlined Auger final states, and in particular, on those in which the shakeup electron acts as a spectator. This result accounts

Table 2

H_2O XPS satellite results (ΔE is the energy shift in eV from $2a_1^{-1}$ peak; I is the percent intensity of $2a_1^{-1}$ peak, i.e. $2a_1^{-1} = 0/100$)

Shakeup feature	$\Delta E / I$				
	a)	b)	c)	d)	e)
$(2 \rightarrow 3)$ $3a_1 \rightarrow 4a_1$	17.07*	19.76	16.00	17.35	14.86
	0.61	3.6	0.15	2.1	2.1
$(4 \rightarrow 5)$ $1b_1 \rightarrow 2b_1$	20.08	22.51	22.02	20.38	19.88
	1.17	0.5	1.37	0.2	0.3
$(6 \rightarrow 7)$ $1b \rightarrow 2b_2$	23.57	22.46	24.72	26.56	24.22
	3.33	0.5	4.3	6.4	10.9
(8) $3a_1 \rightarrow 5a_1$	24.54	23.45	22.93	27.19	
	0.97	5.2	1.32	0.4	
(9) $3a_1 \rightarrow 6a_1$	25.30				
	1.66				
$(12 \rightarrow 13)$ $3a_1 \rightarrow (7a_1, 8a_1)$	28.42				
	1.83				
(14) $1b \rightarrow 4b_1$	35.84				
	0.22				

a) Arneberg et al. [11]. SCF CI sudden approximation (1700 ionic configurations); numbers at left refer to fig. 4b.

b) Wahlgren [69]; equivalent cores-improved virtual-orbital technique.

c) Svensson et al. [70], open shell SCF and internal CI calculation.

d) Cederbaum et al. [71]. 2ph-TDA Green's function with boson approximation (assignments above are indefinite).

e) Creber et al. [72]. Xα-SW calculations.

Table 3
Summary of possible initial core and final Auger states in H_2O

Initial state (excitation energy, eV)	Final states [a]			% Auger [c]
	VO spec. [b]	VO part. [b]	VO shakeoff [b]	
$1a_1^{-1}4a_1$	$n^{-2}4a_1$	n^{-1}	n^{-2}	42
(534.2)	$\underline{b^{-1}n^{-1}4a_1}$	b^{-1}	$\left.\begin{array}{l}\underline{b^{-1}n^{-1}}\\ \underline{b^{-2}}\end{array}\right\}$	58
	$\underline{b^{-2}4a_1}$			
$1a_1^{-1}R$	$n^{-2}R$	n^{-1}	n^{-2}	42
(536–540)	$\underline{b^{-1}n^{-1}R}$	b^{-1}	$\left.\begin{array}{l}\underline{b^{-1}n^{-1}}\\ \underline{b^{-2}}\end{array}\right\}$	58
	$\underline{b^{-2}R}$			
$1a_1^{-1}kl$	n^{-2}			42
(539.9)	$\underline{b^{-1}n^{-1}}$		$\left.\begin{array}{l}\\ \\ \end{array}\right\}$	58
	$\underline{b^{-2}}$			
$1a_1^{-1}A^{-1}B$ [d]	$n^{-2}A^{-1}B$	$n^{-1}A$ [e]	$n^{-2}A^{-1}$	42
(> 550 eV)	$\underline{b^{-1}n^{-1}A^{-1}B}$	$\underline{b^{-1}A}$	$\left.\begin{array}{l}\underline{b^{-1}n^{-1}A^{-1}}\\ \underline{b^{-2}A^{-1}}\end{array}\right\}$	58
	$\underline{b^{-2}A^{-1}B}$			

[a] n, b, and R represent non-bonding, bonding, and Rydberg orbitals respectively; hence $n = (1b_1$ or $3a_1$), $b = (1b_2$ or $2a_1$), and $R = $ any virtual orbital (VO) other than the antibonding $4a_1$ valence orbital. Underlined states are expected to result in H_2O dissociation in ice.

[b] The initial state can decay via three different processes: (1) the virtual-orbital electron can remain as a spectator (VO spec.), (2) the virtual-orbital electron can participate in the Auger process (VO part.), or (3) the virtual-orbital electron can suffer shakeoff along with the Auger process (VO shakeoff). They are believed to be listed in the order of importance, i.e. (1) > (2) > (3).

[c] Percent of the total Auger intensity attributed by the indicated process. See text for further explanation.

[d] $1a_1^{-1}A^{-1}B$ represents any of the ionization plus shakeup excitations, i.e. $1a_1^{-1}3a_1^{-1}4a_1$, $1a_1^{-1}1b_2^{-1}2b_2$ or $1a_1^{-1}n^{-1}R$.

[e] $n^{-1}A$ should be underlined for the case $1a_1^{-1}1b_2^{-1}2b_2$.

for the sharp shoulder at 534 eV in the PSD D^+ yield (i.e. the $1a_1^{-1}4a_1$ PSD intensity is enhanced) and the larger PSD intensity above 550 eV compared the TPY spectrum. The ratios of the 558 eV peak intensity to the 536 eV peak intensity in the PSD and TPY spectra are $(I_{558}/I_{536})_{PSD} \approx 0.7$ and $(I_{558}/I_{536})_{TPY} \approx 0.5$. These ratios are qualitatively consistent with the results in table 3.

The difference between the PSD and TPY spectra below 540 eV has been previously attributed to another mechanism [5]. This mechanism involves differences in broadening of the virtual orbitals depending on the molecular coordination. In this context, the PSD spectrum is interpreted as reflecting the electronic structure of surface molecules, which may be expected to undergo lower coordination and hence reduced broadening. On the other hand, the TPY spectrum is regarded as reflecting bulk-like electronic structure and hence greater peak broadening. This differential virtual-orbital broadening mechanism cannot be ruled out here, but it seems doubtful whether this mechanism can account for the much larger peak intensity in the PSD spectrum around 532 eV, and it definitely does not account for the larger intensity above 550 eV. The differential final state decay mechanism, proposed in this work, accounts for the larger PSD intensity in both energy regions.

The conclusions above were arrived at for $H_2O(s)$. Since the interaction with the adsorbate for molecularly chemisorbed systems is relatively weak, they are believed to be appropriate also for these systems, although no experimental core-level PSD data for $(H_2O)_m/M$ have been reported. The

larger relaxation energy, apparent from the re-
duced 1π and 3σ binding energies in fig. 2, sug-
gests a stronger interaction between OH and Ti.
Indeed, the reduced binding energy may reflect a
metal to OH charge transfer as a result of the
valence ionization. A large charge transfer in the
Auger final state may substantially reduce U^e, and
drastically reduce the OH dissociation cross sec-
tion. This effect is experimentally observed for
chemisorbed CO and NO [73]. No core-level PSD
data are available for OH/Ti.

3.2. Valence-level excitation

As one might expect, the dissociation of $H_2O(g)$
as a result of valence excitation has been exten-
sively studied utilizing a variety of experimental
techniques. These studies include dissociative pho-
toionization of H_2O [8,9,94], dissociative excita-
tion of H_2O by electron impact [75], dissociative
ionization of H_2O by electron impact [76], dissoci-
ation as a result of He⁺ impact at near thermal
energies [77], ultraviolet emission in $O^+ + H_2$ reac-
tive scattering [78], and (e, 2e) and (e, e + ion)
studies [10]. These data complement each other,
and are in surprisingly good agreement. Only the
more recent and complete (e, 2e) and (e, e + ion)
data are presented in fig. 5 [10]. The
$OH(A^2\Sigma^- - X^2\Pi)$, H(Balmer β), and $O(3p^3P -
3s^3S°)$ emission cross sections as a function of
electron-impact energy are in surprisingly good
agreement with the data in fig. 5, which indicates
that excitation into Rydberg states produces dis-
sociation via a mechanism very similar to that for
ionization [75]. From plots of the appearance
potentials (AP) of H⁻ ions as a function of their
kinetic energy (KE), Appell and Durup [76] di-
vided the H⁻ production from electron impact
into six ion groups. These are summarized in table
4 and compared with the electron-coincidence re-
sults from fig. 5.

The assignments of Appell and Durup were
made primarily on the basis of a correlation dia-
gram [78] such as that in fig. 6 and the H_2O^+
potential curves such as that in fig. 7a. These
indicate the excitation energy of the excited states
in the ground-state Franck–Condon region. The
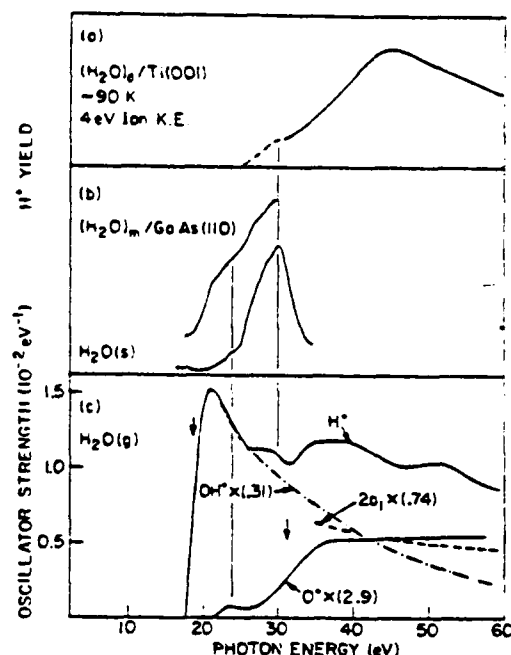excitation probability of the excited states, or the

Fig. 5. (a) PSD H⁺ ion yield for H_2O on Ti(001) at 90 K as
reported in ref. [7]. The H_2O apparently dissociates on the Ti
surface at this temperature. (b) Comparison of the PSD H⁺-ion
yield for molecular H_2O on GaAs(110) and condensed (solid)
H_2O as reported in refs. [6,4] respectively. (c) Oscillator
strengths for ion production (H⁻, OH⁺ or O⁺) as determined
by (e, 2e) and (e, e + ion) data [10]. The OH⁺ and O⁻ oscillator
strengths have been normalized by experimentally-determined
fragmentation ratios H⁻/OH⁺ and H⁺/O⁺ respectively for
easy comparison [10]. The normalized (H⁺/total ions) $2a_1$
branching ratio is also indicated [10]. The vertical arrows
indicate the $1b_2$ and $2a_1$ binding energies.

probability for alternative decay of these excited
states, was not quantitatively considered. Further-
more, the apparent AP energies from electron
impact are consistently smaller than those ob-
tained from the coincidence data in fig. 5. This
discrepancy in energy is believed to be primarily
responsible for the difference in assignments be-
tween Appell and Durup and those preferred here.
Nevertheless, the importance of the 2b1e states is
realized already in their work.

There is no doubt about the $(1b_2^{-1})^2B_2$ assign-
ment for the first contribution with AP in the
region 18–21 eV. This assignment is confirmed by
the similarity of the $1b_2^{-1}$ partial oscillator strength,
and the OH⁺- and H⁺-ions yields in this region

Table 4

Electron impact and (e, 2e)-(e, e + ion) results for H^+ production from H_2O

Ion group A → D[a]	KE (eV) range A → D[a]	AP (ev) range A → D[a]	Preferred assignment A → D[a]	AP (eV) range, fig. 5	KE (eV) (e, e + ion)[c]	Preferred assignment this work
1	0–1.2	18.7–21	$(1b_2^{-1})^2B_2$	18–21	0.14	$(1b_2^{-1})^2B_2$
2–4	0–4.0	20.7–24	$1b_1^{-1}3a_1^{-1}R4a_1$	21–25		$(1b_1^{-1}3a_1^{-1}4a_1)^2B_1$
5	4.0–7.0	23.4–27.5	$(1b_1^{-1}3a_1^{-1}4a_1)^2B_1$	26–31		$(1b_1^{-2}4a_1)^2A_1$
6	1.0–4.2 [b]	27.0–31.5	$(1b_1^{-1}3a_1^{-1}4a_1)^2B_1$ or $(1b_1^{-2}4a_1)^2A_1$	31–36		$(2a_1^{-1})^2A_1$
				47–51		double ionization [c]

[a] Appell and Durup ref. [76].

[b] Ehrhardt observed a range from 1–7 eV for this contribution [75].

[c] Ref. [10].

(see fig. 5) [10]. The dissociation must result from a predissociation process, since the $(1b_2^{-1})$ $^2B_2$ potential curve itself is attractive at these energies [79]. The predissociation results from the curve crossings with the $(1b_1^{-1}3a_1^{-1}4a_1)$ $^2B_1$ and $^4B_1$ states, which correlate with the $OH(X\,^2\Pi)+H^+$ and $OH^+(X\,^3\Sigma^-)+H$ fragments respectively, con-

sistent with the production of OH^+ and H^+ ions (figs. 6 and 7). A curve crossing also occurs with an $^4A_2$ state, which correlates to $O^+(^4S_u)+H_2$ fragments and provides for O^+ production; however, little O^+ production is seen in this region. This is apparently because this curve crossing oc-

Fig. 6. Correlation diagram for pertinent states of H_2O^+ as obtained from ref. [78]. The states which correlate to the $2a_1^{-1}$ ^2A state are not certain, however the fragmentation data suggest it correlates to $O^- + H_2$ and $OH + H^+$ like states [10].

Fig. 7. Comparison of some of the pertinent theoretical potential curves for H_2O^+ and OH [49,93]. The H_2O states are labeled according to the C_s point group. The H_2O and OH energy scales have been shifted so that the potential minimum of the $(1b_1^{-1})^2A''$ and $(1\pi^{-1})$ $^2\pi$ curves align with the corresponding experimental ionization energies in $H_2O(g)$ and OH/Π respectively. The experimental $(2a_1^{-1})^2A'$ and $(2\sigma^{-1})^2\Sigma$ ionization energies are also indicated.

curs far from the FC region making it an improbable event [30–37]. A most important observation from the point of view of this work is the slow rate (10^9 s^{-1}) of the predissociation process as determined from theoretical calculations [80]. It is many orders of magnitude less than the rate (10^{12}–10^{13} s^{-1}) for direct dissociation from a repulsive potential curve. Nevertheless, in the gas phase where no other decay mechanisms exist, the process occurs with high probability. This is not the case in condensed systems as will become evident below.

The H$^-$ contributions with AP equal to 21–25 eV and 26–31 eV in fig. 5 are assigned here to the ($1b_1^{-1}3a_1^{-1}4a_1$) $^2B_1$ and ($1b_1^{-2}4a_a$) $^2A_1$ 2h1e states. These two states are those in table 1 with an excitation energy significantly below the $2a_1^{-1}$ state, as discussed in section 2. Whereas the AP (fig. 2) and the binding energy (table 1) for the $1b_1^{-2}4a_1$ state align properly, the binding energy of the ($1b_1^{-1}3a_1^{-1}4a_1$) $^2B_1$ state, estimated to be around 28 eV from the SCF calculations of Leclerc et al. [49], is significantly above the 21–25 eV AP. This fact lead Appel and Durup to suggest the involvement of the Rydberg states, $1b_1^{-1}3a_1^{-1}4a_1R$, converging to this same ionic state [76]. However, the calculations of Leclerc et al. do not include electron-correlation effects, which might lower the binding energy of the ionic state by 2 or 3 eV [49]. The ($1b_1^{-1}3a_1^{-1}4a_1$) $^2B_1$ state does correlate to the proper H$^-$ + OH(X $^2\Pi$) and O$^+$(^2D) + H$_2$ fragments, providing a direct mechanism for the observed O$^-$ and H$^+$ ions in this region. The relative magnitudes of the 21–25 and 26–31 eV H$^-$ contributions are also consistent with these two assignments. Nevertheless, until further calculations are reported, the $^2B_1$ assignment will remain somewhat uncertain.

The H$^-$ contribution with AP of 31–36 eV (fig. 2) is assigned to the ("$2a_1^{-1}$") $^2A_1$ state consistent with the 32 eV binding energy of this state (fig. 2). Fig. 5 also compares the $2a_1$ CIS photoelectron yield with the O$^-$ yield above 35 eV [10]. They are both in good agreement with the H$^+$ yield between 32 and 57 eV confirming this assignment. Although Appel and Durup [76] mentioned the $2a_1^{-1}$ state as a source for their ion group 6, it was ruled out on the basis of their observed AP of 27–31.5

eV, which is 4 eV below the value determined from the coincidence data in fig. 5. It must also be mentioned here again that the $2a_1^{-1}$ configuration mixes heavily with many 2h1e configurations (table 1 and fig. 2), so that here the entire group of states is referred to as the "$2a_1^{-1}$" spectroscopic state.

Finally, the appearance of an additional H$^-$ contribution with AP around 47–51 eV has been observed only in the coincidence data. It has been attributed to dissociative double ionization [10] (or ionization plus shakeoff).

Comparison of the ion-yield spectra for H$_2$O(s) [4], (H$_2$O)$_m$/GaAs [6], and (H$_2$O)$_a$/Ti [7], with that for H$_2$O(g), reveals some dramatic differences. Most important, primarily H$^+$ ions are observed from these condensed-phase systems. Very little OH$^+$, O$^+$, or even H$_2$O$^-$ (e.g. H$_2$O$^+$/H$^+$ < 1000) is seen [7], although H$^+$(H$_2$O)$_n$ cluster ions have been observed at higher temperatures (e.g. clusters of from 1 to 9 water molecules have been observed from H$_2$O(s) at 193 K) [83]. The latter phenomenon has been interpreted in terms of H$_2$O clustering about an energetic H$^-$ ions. Presumably the escape probability of these very heavy H$^+$(H$_2$O)$_n$ ions is negligible at lower temperatures because of an increased potential barrier. This may arise from an observed decrease in the conductivity and increased negative surface charging of the ice surface [83]. The near lack of OH$^-$ and O$^-$ ions from all of the condensed systems is believed to arise from the large competitive excited-state decay rates, which decrease the escape probability of the heavier (relative to H$^-$) ions [2]. These decay phenomena arise from intermolecular covalent bonding interactions (i.e. adsorbate–substrate or H-bonding interactions), which allow intermolecular charge transfer such as resonant charge transfer or one and two hole hopping (reneutralization) [1–3]. The latter is consistent with an isotope effect observed in several systems [84].

Fig. 5 compares the H$^-$ ion-yield spectra for the condensed phases with that for H$_2$O(g). The absence of the $1b_2^{-1}$ contribution in all three condensed phases is most conspicuous. This arises because of the slow $1b_2^{-1}$ predissociation rate [80] ($\approx 10^9$ s^{-1}) compared with the intermolecular de-

cay rates [3] ($\approx 10^{12}$ s^{-1}) mentioned above. The ions yields for (H₂O)$_m$/GaAs and H₂O(s) have not been reported for energies above 30 and 35 eV respectively, thus contributions above these energies (e.g. from the 2h states) cannot be ruled out. Nevertheless it seems that the "2a$_1^{-1}$" contribution with threshold at $\approx$ 32 eV does not appear in the condensed phases except possibly for (H₂O)$_d$/Ti. This may occur because of the absence of H bonding in the latter system for less than monolayer coverages, although other interpretations are discussed below. For (H₂O)$_m$/GaAs and H₂O(s). the broadening of the a₁ bands (as indicated in section 2) increases the "2a$_1^{-1}$" width, and hence the intermolecular hopping rate. The 2h1e contributions at 24 and 31 eV appear in all three condensed phases. Apparently the intermolecular hopping rates are not as large in these three particle states [3]. Some reduction in the H$^-$-ion yield from these 2h1e states is apparent however, particularly for small coverages on metal surfaces [7.39].

4. Discussion

4.1. The H₂O(s) and (H₂O)$_m$/GaAs ion yields

Several items should be mentioned concerning the spectral line shapes of the ion yields. First, the fine structure seen in the 2h1e contributions of the H₂O(s) and (H₂O)$_m$/GaAs ion yield spectra is apparently real, i.e. it is reproducible. Its source is not clear. The structure between 21 and 24 eV in the (H₂O)$_m$/GaAs spectrum is similar to that observed in the secondary electron yield (SE yield) and in the reflectance spectrum from GaAs(110) [6]. These latter spectra are believed to mirror the density of states of the conduction band (CB) in bulk GaAs, since the spectra are interpreted as arising from Ga3d$_{3/2,5/2} \to$ CB transitions [6]. From this information. Thornton et. al. [6] concluded that the H$^+$ ions arise not from intramolecular 2h1e excitations in the H₂O molecule, but from an Auger-type mechanism involving the Ga3d$_{3/2,5/2}$ substrate core levels. They also indicated dissociative adsorption of H₂O on GaAs(110). forming Ga-H bonds. This was neces-

sary to explain the H$^+$ desorption as a result of the Ga core-level excitation indicated above. Three facts argue against this interpretation: (1) two additional peaks at $h\nu$ = 19.3 and 19.8 eV in the SE yield have been attributed to Ga3d$_{3/2,5/2} \to$ surface exciton transitions; these peaks are not present in the H$^+$ yield spectrum [6]. (2) the UPS spectrum indicates the H₂O is not dissociated (section 2), and (3) the similarity of the fine structure in the H₂O(s) and (H₂O)$_m$/GaAs H$^-$-ion yields indicates the fine structure arises from a source other than the GaAs conduction band states. Since this fine structure is apparently absent in H₂O(g), it may arise in the condensed phases from the intermolecular H bonding (i.e. reflecting the H₂O "conduction band" states).

4.2. The (H₂O)$_d$/Ti ion yield

The similarity between the H$^+$-yield thresholds from (H₂O)$_d$/Ti and from the molecular H₂O systems is perhaps surprising in light of the UPS spectra which showed relatively large differences. The potential curves for H₂O and OH are very similar however, as compared in fig. 7. Note that the curves for OH are given rather than for OH$^+$ [85]. This allows a more direct comparison between the curves, since both systems contain a single valence hole and hence have the same multiplet states. OH is also more appropriate than OH$^+$, since some charge transfer from the absorbate probably occurs in the case of OH/M. In any event, the OH valence orbitals of the OH/Ti system are fully occupied like in OH$^-$.

The H₂O curves in fig. 7 are obtained from LCAO MO SCF calculations [49]; they compare favorably with more limited but more accurate results for H₂O in the literature [86–92]. The OH curves are obtained from AO CI results [93]; they also compare semi-quantiatively with more limited but comparable results for OH [94–96]. The excitation energies of these potential curves have been scaled so that the (1b$_1^{-1}$) ^{2}A″ and (1π^{-1}) $^2\Pi$ states agree with the experimental first ionization potentials in H₂O and OH/Ti respectively (fig. 2). Potential curves for either the (2a$_1^{-1}$) ^{2}A state in H₂O or the (2σ^{-1}) $^2\Sigma$ in OH are not available, and only the experimental energy in the ground-

state FC region is given in each case (fig. 2). All of the 2h1e states are repulsive in each case, indicating their possible effectiveness in dissociation. The $(1b_1^{-2}4a_1)$ $^2A''$ state in H_2O has an excitation energy of $\approx$ 27–28 eV in the FC region, which is consistent with fig. 5. The $(1b_1^{-1}3a_1^{-1}4a_1)$ $^2A''$ and $^2A'$ potential curves lie below the $(1b_1^{-2}4a_1)$ $^2A''$ curve in the FC region, which is also consistent with fig. 5. According to fig. 7, the $1\pi^{-2}4\sigma$ potential curves have energies just below 20 eV in the FC region, which is lower than that indicated in fig. 5a; however, the strong bonding of the OH with the Ti is not accounted for in these gas-phase potential curves. Note that the $(1b_1^{-2}4a_1)$ ^2A and $(1b_1^{-1}3a_1^{-1}4a_1)$ states of H_2O merge into the $(1\pi^{-2}4\sigma)$ states of OH, thus only one 2h1e contribution is expected for OH/Ti as observed.

The similarity of the PSD ion yield thresholds and relative peak intensities from OH/Ti and $H_2O(g)$ provide a strong argument for the $1\pi^{-2}4\sigma$ and "$2\sigma^{-1}$" assignments with thresholds at $\approx$ 23 and $\approx$ 33 eV respectively. However, the difference above 33 eV in the ion-yield spectral lineshape from these two systems cannot be ignored. Indeed, the H^--ion yield profile from OH/Ti above 35 eV is remarkably similar to the O^--ion yield from O_2/Ti and the SE yield spectrum from Ti [97]. Based on this comparison, Stockbauer et al. [7] attributed the H^+ yield above 33 eV to an Auger mechanism involving the Ti 3p core level, and assigned that around 23 eV to the Auger mechanism involving the 2σ level. Their assignments are supported by Weng and Kammerer [97] who found similar ESD H^--ion yield thresholds from a mixture of H_2 and H_2O adsorbed on O contaminated Nb(100) and Ta(110). In his work two thresholds were also found, one at $\approx$ 22 eV yielding 2 eV H^+ ions and attributed to the O(2s) core level; the other at 28 (31) eV giving 6 (4) eV ions and attributed to the Ta 4f (Nb 4p) core level at 25 (33) eV. In contrast to Stockbauer et al. [7] Weng and Kammerer suggested that the 28 (31) eV threshold may result from H–M bonds rather than from OH species.

Support for the $1\pi^{-2}4\sigma$ and "$2\sigma^{-1}$" assignments, on the other hand, can be obtained from other data. The PSD H^+-ion yield from $(H_2O)_d$/Ti is similar in many respects to the O^--ion yield

from CO/Ru [97]. In CO/Ru, the initial O^+ threshold occurs around 22 eV and is attributed to the $5\sigma^{-2}6\sigma$ state, followed by a much larger contribution at 29 eV attributed to the "$3\sigma^{-1}$" state [1]. The $5\sigma^{-2}6\sigma$ and "$3\sigma^{-1}$" states in Co are directly comparable to the $1\pi^{-2}4\sigma$ and "$2\sigma^{-1}$" states in OH. No Ru-core levels exist around 29 eV, so no uncertainty exists as to the "$3\sigma^{-1}$" assignment for CO/Ru [1]. The ESD of H^- ions from "SiOH" also revealed thresholds at 20 and 33 eV [99], where again no Si-core levels exist, yet these two thresholds are comparable to those found for OH on Ti, Nb and Ta. The similarity of the H^+ threshold energies, in spite of the changing Ti, Nb, and Ta core-level energies in this region, also suggests that the core levels are not involved here. Finally, the H^+-ion kinetic energies obtained from OH on Ti, Nb, and Ta, which are dominated by the contribution with threshold at 28–33 eV, have a broad distribution extending from 0 to 7–9 eV and peaks around 3.5–6 eV [98,7]. This is similar to that obtained from dissociation of $H_2O(g)$, where the dominant contribution definitely arises from the "$2a_1^{-1}$" final state [76].

The similarity of the H^+ spectral lineshape from OH/Ti above 33 eV to both the O^+-ion yield from O_2/Ti and the SE yield spectrum from Ti provides a strong argument for the O(2s) and Ti(3p) assignments [97]. Furthermore, the desorption thresholds at 22 and 33 eV align nicely with the O(2s) and Ti(3p) binding energies (relative to the Fermi energy) [7,97]. How can these facts be accounted for consistently within the $1\pi^{-2}4\sigma$ and "$2\sigma^{-1}$" assignments suggested in this work? Consider first the "$2\sigma^{-1}$" binding energy question. Relative to the Fermi level, the "$2\sigma^{-1}$" binding energy falls around 24 eV, much closer to the 23 eV threshold than the 33 eV threshold. But in $H_2O(g)$, the "$2a_1^{-1}$" binding energy is around 32 eV relative to the vacuum. This difference is due of course to an $\approx$ 5 eV work function and an $\approx$ 2–3 eV relaxation shift. It is important to realize however that the "$2\sigma^{-1}$" photoionization spectral profile does not shift accordingly. To first approximation, the presence of the Ti substrate merely allows ionization to occur at a lower energy; its ionization threshold is shifted (e.g. in fig. 4d, the $1a_1$ ionization threshold indicated by the hatched line merely shifts to

lower energy on the same spectral lineshape). Thus excitations from the O(2s) orbital to the Rydberg or virtual orbitals, which in H_2O(g) may result in neutral dissociation (H + OH) or no dissociation [50], now results in ionization which may yield H^+ desorption. This suggests the possibility that the 22 eV contribution in fig. 5a may result from 1h1e states (e.g. $2\sigma^{-1} 4\sigma$ states) rather than the 2h1e states; however, this is unlikely because calculations in H_2O(g) indicate that the $2a_1^{-1}$ excitation is unique in this instance [50]. The Rydberg and virtual-orbital excitations from the $2a_1^{-1}$ are much weaker than from the upper valence or $1a_1$ orbital (i.e. peaks 1–4 in fig. 4d are an order of magnitude smaller in the $2a_1^{-1}$ photoionization cross section) [50]. This suggests that although the "$2\sigma^{-1}$" O^+-ion yield may extend down to 22 eV, it decreases uniformly with decreasing energy in the 22–33 eV region, with the peak at 30 eV arising from the 2h1e states.

In addition to the shift in ionization threshold, the presence of the Ti may alter the "$2\sigma^{-1}$" photoionization lineshape. Calculations [50] and experiment (fig. 5c) for H_2O(g) indicate that the broad and unstructured ($2a_1^{-1}$) $^2A_1$ photoionization profile is generally O 2s → kp like with the H atoms having little effect. However, strong O–Ti interactions may alter the "$2\sigma^{-1}$" profile by the introduction of a resonance, or other structure, making it appear more like the SE yield from Ti and O^- yield from O_2/Ti, since all three under these circumstances mirror the final density of states of the Ti–O (or Ti–OH) system. Finally, the Ti to OH charge transfer which occurs upon ionization of OH (section 2), may introduce large shakeup transitions similar to those discussed in section 3 for the O K level in H_2O(g). This would have the effect of increasing the ion-desorption yield ≈ 20 eV above threshold as discussed in section 3, and thus may also contribute to the peak around 40 eV in the OH/Ti PSD H^+ yield.

It seems clear the further work is required to be definite on the assignments of the two H^+-ion yield peaks from $(H_2O)_d$/Ti. If indeed the Ti core level is involved in the H^+-ion yield, it would be most interesting. The PSD H^+-ion yield is obtained only in the presence of OH (i.e. H/Ti or H/Ti – coadsorbed O does not give a PSD H^+

yield [7], yet to date no other instance is reported where desorption of a fragment ion arises from the excitation of an atom which is not bonded to or part of the desorbing fragment [7]. Nevertheless, this mechanism cannot be ruled out on this basis. Indeed, both the O(2s) and Ti(3p) excitations could both be partially responsible for the larger H^+ contribution above 33 eV. This work assumes the 2h1e and "$2\sigma^{-1}$" assignment for the reasons indicated above.

8.3. The "$2a_1^{-1}$" desorption mechanism

In the context of discussing the "$2a_1^{-1}$" (or "$2\sigma^{-1}$") ion contribution [its presence is indicated in either assignment above and it definitely arises in H_2O(g)], the "$2a_1^{-1}$" desorption or dissociation mechanism should be discussed. The $1b_2^{-1}$ state predissociates, the 2h1e states are clearly repulsive, but the desorption mechanism of the $2a_1^{-1}$ state is not clear. It was indicated in section 2 that the $2a_1^{-1}$ state contributes only ≈ 20% to the total H–O bond energy, and that generally it is characterized as a core orbital. Definitely the $2a_1^{-1}$ potential curve is not repulsive, but it may be shifted sufficiently so that a FC excitation from the ground state results in an excitation energy above the $2a_1^{-1}$ dissociation limit (the MGR mechanism). As indicated above, the theoretical $2a_1^{-1}$ potential curve is not available in the literature.

The strong mixing with the more repulsive 2h1e states, which occurs in a full CI calculation, may be much more instrumental in bringing about the "$2a_1^{-1}$" H^+ contribution. In particular, the highly repulsive $3a_1^{-2}4a_1$ state is the nearest in energy to the $2a_1^{-1}$ configuration and undergoes the heaviest mixing. Let us assume for the purpose of this discussion that these are the only two states involved, thus

$$\psi_1 = N(2a_1^{-1} + c3a_1^{-2}4a_1),$$

$$\psi_2 = N(c2a_1^{-1} - 3a_1^{-2}4a_1).$$

When c equals zero, neither state ψ_1 nor ψ_2 results in desorption because ψ_1 must then produce desorption via the MGR mechanism which we assume is not active, and ψ_2 is not excited because

the $3a_1^{-2}4a_1$ photoexcitation cross section is zero. As c increases. ψ_1 becomes more repulsive and ψ_2 gains an increased excitation yield. As c approaches one. both ψ_1 and ψ_2 may produce desorption almost equally. Thus CI mixing is very instrumental in the desorption process with the dissociation mechanism a 2h1e process and the excitation mechanism a $2a_1^{-1}$ one-electron excitation. In this picture the "$2a_1^{-1}$" contribution is really a $3a_1^{-2}4a_1$ 2h1e contribution like the other 2h1e contributions. Hydrogen bonding apparently broadens all a_1 orbitals [26.27] so that the $3a_1^{-2}4a_1$ and $2a_1^{-1}$ states. and mixtures of them. become sufficiently short lived to abort the desorption process. The $3a_1^{-1}1b_1^{-1}4a_1$ and $1b_1^{-2}4a_1$ 2h1e states involve only one or no holes in the $3a_1$ orbital, so hydrogen bonding does not affect these states as dramatically.

At least three other desorption mechanisms have been suggested for the "$2a_1^{-1}$" contribution. Assuming the $2a_1^{-1}$ state is core-like. Auger decay might be expected to result in H^- desorption similar to the KF type mechanism [7]. However, the $2a_1^{-1}$ state does not have sufficient energy for Auger decay since the lowest 2h state has a larger excitation energy [100]. Laramore [66] theoretically estimates the lowest 2h state $(3a_1^{-1}1b_1^{-1})$ to have an energy ≈ 5 eV above the $2a_1^{-1}$, the large energy resulting from a ≈ 10 eV hole–hole repulsion, U^e. The coincidence data in fig. 5 also indicate that 2h contributions appear significantly above the $2a_1^{-1}$ energy [10]. Recently. Laramore [66] suggested a resonant Auger-type process might occur to the $3a_1^{-2}4a_1$ state. which then dissociates. Laramore suggests this state lies 1.4 eV below the $2a_1^{-1}$ state; this can be compared with the CI results in table 1, which indicates a value more like 4–5 eV. In any event. the excess energy of the $2a_1^{-1}$ state must be absorbed by the non-electronic degrees of freedom. such as vibration and rotation. if the resonant Auger process is to occur. Finally. an essentially identical mechanism to the 2h1e CI mixing mechanism has been proposed by Melius et al [101] but discussed in the language of predissociation. In this context. the many 2h1e states above the $2a_1^{-1}$ state in the FC region may enter. since the 2h1e states are generally more repulsive than the $2a_1^{-1}$ state. It follows that the 2h1e potential

curves probably cross the $2a_1^{-1}$ curve at larger internuclear separation. allowing for the predissociation via an internal conversion process.

Which of the five described mechanisms seems most feasible at this point? The MGR mechanism is not considered feasible. The normal Auger mechanism is eliminated from consideration by the energy arguments above. The resonant Auger. the CI mixing. and the predissociation mechanism all involve the 2h1e states, however the mechanisms for excitation of the 2h1e states are different. The resonant Auger and predissociation mechanisms involve the nuclear degrees of freedom such as vibration and rotation to produce a "resonant" process (i.e. to either absorb an excess kinetic energy or produce the curve crossing). The inclusion of the nuclear degrees of freedom suggests relatively slow processes with rates of the order of the desorption process itself. The CI mixing process is instantaneous, and is therefore reflected in the XPS "sudden" limit for shakeup. It is impossible at this point to determine that one mechanism is dominant over the other, but it is clear that the CI mixing mechanism is responsible for the $3a_1^{-1}1b_1^{-1}4a_1$ and $1b_1^{-2}4a_1$ contributions at 22 eV, since they are reflected by the shakeup satellites. Therefore. it does not seem necessary at this point to invoke another mechanism for the "$2a_1^{-1}$" contribution.

5. Summary and conclusions

The results of this work can best be summarized by fig. 8. It indicates the branching and fragmentation patterns for H_2O in the various phases studied. and assumes the "$2\sigma^{-1}$" contribution as discussed above for OH/Ti. Quantitative fragmentation ratios for $H_2O(g)$, as obtained from electron coincidence experiments [10] are also indicated.

The following conclusions can be drawn from this work.

(1) The $1b_2^{-1}$ state, which fragments $H_2O(g)$ via a predissociation mechanism, is not effective in the condensed systems because of faster intermolecular decay mechanisms for the $1b_2^{-1}$ state.

(2) Excitation of the "$2a_1^{-1}$" state produces a large H^+ contribution in $H_2O(g)$ and perhaps the
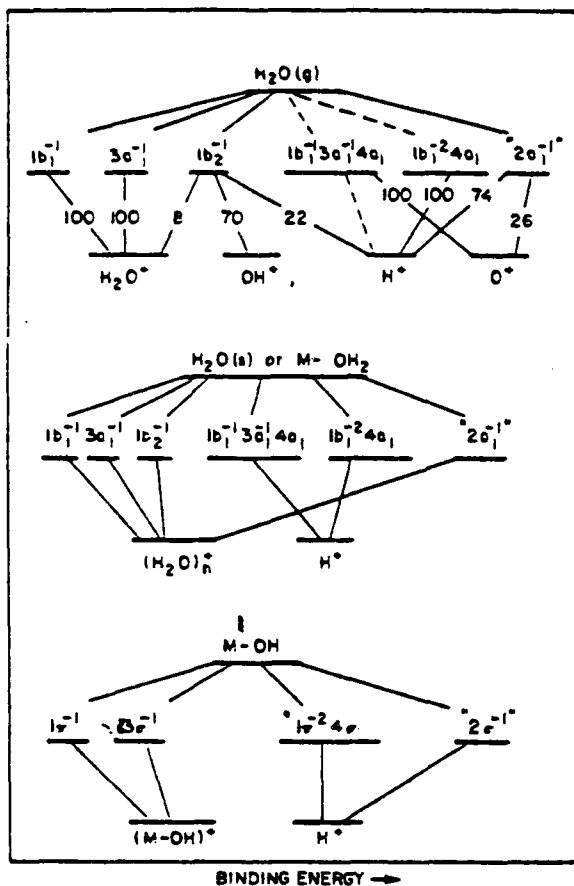
BINDING ENERGY →

Fig. 8. Summary of PSD results for $H_2O(g)$, $H_2O(s)$, and molecularly chemisorbed and dissociated H_2O on metals (e.g. OH on Ti assuming the contribution above 32 eV arises via the "$2\sigma^{-1}$" excitation). The various excited states are indicated in order of increasing excitation energy. For $H_2O(g)$, the experimental fragmentation ratios are indicated [10]. Dotted lines indicate small contributions (i.e. small branching or fragmentation ratios). $(H_2O)_n^*$ or $(M-OH)^+$ indicate no desorption.

"$2\sigma^{-1}$" for OH/M, but the actual desorption mechanism is not clear. Hydrogen bonding eliminates the "$2a_1^{-1}$" contribution in $H_2O(s)$ or H_2O/M by again providing an increased intermolecular hole hopping rate.

(3) The 2h1e mechanism is the only active mechanism in the condensed hydrogen-bonded systems, however evidence does exist indicating that the absorbate–substrate interactions may also

reduce the 2h1e-ion yield.

(4) Whether the 2h1e state is excited by core hole Auger decay, or by CI mixing, occupation of the $4a_1$ antibonding virtual orbital (i.e. $1e = 4a_1$) is critical to the desorption process.

Comparison of these results for H_2O with previous results for CO reveals they are surprisingly similar [1–3]. The following correlations can be made.

(1) The active 2h1e states, $1b_1^{-2}4a_1$ and $3a_1^{-1}1b_1^{-1}4a_1$, in H_2O are comparable to the $5\sigma^{-2}6\sigma$ state in CO.

(2) The $2a_1^{-1}$ state in H_2O is comparable to the $3\sigma^{-1}$ state in CO. In the gas phases both produce large ion yields (H^+/H_2O or O^+/CO) but mix in heavily with the 2h1e states.

(3) The $4a_1$ orbital in H_2O is comparable to the 6σ orbital in CO; however here an important difference arises. The 6σ orbital is so antibonding it lies above the continuum threshold, while the $4a_1$ orbital although antibonding lies well below the continuum. Thus resonant decay is not important in H_2O.

(4) Core-level PSD occurs via the Auger process in both the gas and solid phases of CO and H_2O. However, here the chemisorbed CO data are used to predict results for chemisorbed H_2O, since experimental data are not available in the literature. CO and OH are expected to behave similarly, both allowing substrate charge transfer to reduce U^* and reduce the desorption cross section. However, this reduction is expected to be much less dramatic in OH since no empty π orbital exists just above the Fermi level as in CO. In molecularly chemisorbed H_2O, this charge transfer is not believed to be effective so that large core-level PSD is expected.

The results obtained for H_2O can be generalized and extended to other systems. For example, H_2S is expected to behave in a manner similar to H_2O, indeed the H_2S data which is available indicates the presence of the same 2h1e type satellites in the photoemission or (e, 2e) data [102]. Application to various alcohols, such as CH_3OH and C_2H_5OH, is also feasible with certain modifications. Such studies are underway.

References

[1] D.E. Ramaker, J. Chem. Phys. 78 (1983) 2998.

[2] D.E. Ramaker, J. Vac. Sci. Technol. ●●● (1983) ●●●.

[3] D.E. Ramaker, in: Desorption induced by electronic transitions, eds. N.H. Tolk, M.M. Traum, J.C. Tully and T.E. Madey (Springer, Berlin, 1982) p. 70.

[4] R.A. Rosenberg, V. Rehn, V.O. Jones, A.K. Green, C.C. Parks, G. Loubriel and R.H. Stulen, Chem. Phys. Letter 80 (1981) 488.

[5] R.A. Rosenberg, V. Rehn, A.K. Green, P.R. LaRoe and C.C. Parks, in: Desorption induced by electronic transitions, eds. N.H. Tolk, M.M. Traum, J.C. Tully and T.E. Madey (Springer, Berlin, Heidelberg (1982) p. 247.

[6] G. Thornton, R.A. Rosenberg, V. Rehn, A.K. Green and C.C. Parks, Solid State Commun 40 (1981) 131.

[7] R.L. Stockbauer, D.M. Hanson, S.A. Flodstrom and T.E. Madey, J. Vac. Sci. Technol. 20 (1982) 562; Phys. Rev. B 26 (1982) 1885.

[8] R.B. Cairns, 'I. Harrison and R.I. Schoen, J. Chem. Phys. 55 (1971) 4886.

[9] P.L. Kronebusch and J. Berkowitz, Intern. J. Mass Spectr. Ion Phys. 22 (1976\283.

[10] K.H. Tan, C.E. Brion, Ph.E. van der Leeuw and M.J. van der Wiel, Chem. Phys. 29 (1978) 299;
G.R. Branton and C.E. Brion, J. Electron Spectry. 3 (1974)4129.

[11] R. Arneberg, J. Müller and R. Manne, Chem. Phys. 64 (1982) 249.

[12] N.H. Tolk, M.M. Traum, J.C. Tully and T.E. Madey, eds., Desorption induced by electronic transitions (Springer, Berlin, 1982).

[13] D. Menzel and R. Gomer, J. Chem. Phys. 41 (1964) 3311; P.A. Redhead, Can. J. Phys. 42 (1964) 886.

[14] M.L. Knotek and P.J. Feibelman, Phys. Rev. Letters 40 (1978) 946; Surface Sci. 90 (1979) 78; Phys. Rev. B18 (1978);
P.J. Feibelman, Surface Sci. 102 (1981) L51.

[15] D.E. Ramaker, C.T. White ad J.S. Mürday, J. Vac. Sci. Technol. 18 (1981) 748; Phys. Letter 89A (1982) 211.

[16] M.J. van der Wiel, Electron and atomic collisions (North-Holland, Amsterdam, 1980) p. 209;
P.E.M. Siegbahn, Chem. Phys. 66 (1982) 443.

[17] K. Siegbahn et al, K. Siegbahn, C. Nordling, G. Johansson, J. Hedman, P.F. Heden, K. Hamrin, U. Gelius, T. Bergmark, L.O. Werme, R. Manne and Y. Baer, ESCA applied to free molecules (North-Holland, Amsterdam, 1969) p. 83; J. Electron Spectry. 5 (1974) 3

[18] A.J. Yencha, H. Kubota, T. Fukuyama, T. Kendow and K. Kuchitsu, J. Electron Spectry. 23 (1981) 431.

[19] W. von Niessen, G.H.F. Diercksen and L.S. Cederbaum, J. Chem. Phys. 67 (1977) 4124.

[20] M.S. Banna and D.A. Shirley, J. Chem. Phys. 63 (1975) 4759.

[21] B. Baron and F. Williams, J. Chem. Phys. 64 (1976) 3896;
B. Baron, D. Hoover and F. Williams, J. Chem. Phys. 68 (1978) 1997.

[22] J. Abbati, L. Braicovich and B. De Michelis, Solid State Commun. 29 (1979) 511.

[23] M. Watanabe, H. Kitamura and Y. Nakai, in: VUV radiation physics, eds. E.E. Koch, R. Haensel and C. Kunz, (Pergamon, New York, 1974) p. 70.

[24] G.P. Parravicini and L. Resca, Phys. Rev. B8 (1973) 3009.

[25] T. Shibaguchi, H. Onuki and R. Onaka, J. Phys. Soc. Japan 42 (1977) 152.

[26] S. Scheiner, J. Chem. Phys. 75 (1981) 5791.

[27] K. Morokuma and J.R. Winick, J. Chem. Phys. 52 (1970) 1301.

[28] J.N. Miller, D.T. Ling, P.M. Stefan, D.L. Weissman, M.L. Shek, I. Lindau and W.E. Spicer, Phys. Rev. 24 (1981) 1917;
J.N. Miller, I. Lindau and W.E. Spicer, Surface Sci. 111 (1981) 595.

[29] A.B. Anderson, Surface Sci. 105 (1981) 159.

[30] S. Holloway and K.H. Bennemann, Surface Sci. 101 (1980) 327.

[31] T.E. Madey and J.T. Yates, Chem. Phys. Letters 51 (1977) 77.

[32] F. Flores, I. Gabbay and N.H. March, Surface Sci. 107 (1981) 127.

[33] H. Ibach and S. Lehwald, Surface Sci. 91 (1980) 187.

[34] G.B. Fisher and J.L. Gland, Surface Sci. 94 (1980) 446.

[35] B.A. Sexton, J. Vac. Sci. Technol. 16 (1979) 1033.

[36] J.J. Zinck and W.H. Weinberg, J. Vac. Sci. Technol. 17 (1980) 188.

[37] P.A. Thiel, F.M. Hoffmann and W.H. Weinberg, J. Chem. Phys. 75 (1981) 5556.

[38] D.L. Doering and T.E. Madey, Surface Sci. 123 (1982) 231;
E.D. Williams and D.L. Doering, to be published.

[39] T.E. Madey and F.P. Netzer, Surface Sci. 117 (1982) 549;
F.P. Netzer and T.E. Madey Phys. Rev. Letters 47 (1981) 928.

[40] M. Buchel and H. Luth, Surface Sci. 87 (1979) 285.

[41] K. Fujiwara, J. Chem. Phys. 75 (1981) 5172; Surface Sci. 108 (1981) 124;
H. Ibach, H. Wagner and D. Bruchmann, Solid State Commun. 42 (1982) 457.

[42] D.J. Dwyer and G.W. Simmons, Surface Sci. 64 (1977) 617.

[43] J.C. Lorquet and C. Cadet, Chem. Phys. Letters 6 (1970) 198.

[44] A.J. Dixon, S. Dey, I.E. McCarthy, E. Weigold and G.R.J. Williams, Chem. Phys. 21 (1977) 81;
S.T. Hood, A. Hamnett and C.E. Brion, J. Electron Spectry. 11 (1977) 205.

[45] H.A. Agren and H. Siegbahn, Chem. Phys. Letters 69 (1980) 424.

[46] L.S. Cederbaum, Mol. Phys. 28 (1974) 479.

[47] T.E. Madey, unpublished.

[48] M. Mishra and Y. Ohrn, Chem. Phys. Letters 71 (1980) 549.

[49] J.C. Leclerc, J.A. Horsley and J.C. Lorquet, Chem. Phys. 4 (1974) 337.

[50] G.H.F. Diercksen, W.P. Kraemer, T.N. Rescigno, C.F. Bender, B.V. McKoy, S.R. Langhoff and P.W. Lanhoff, J. Chem. Phys. 76 (1982) 1043; G.R.J. Williams and P.W. Langhoff, Chem. Phys. Letters 60 (1979) 201.

[51] C.M. Truesdale, S. Southworth, P.H. Kobrin, D.W. Lindle, G. Thornton and D.A. Shirley, J. Chem. Phys. 76 (1982) 860.

[52] W.C. Tam and C.E. Brion, J. Electron Spectry. 3 (1974) 263.

[53] G.R. Wight and C.E. Brion, J. Electron Spectry. 4 (1974) 25.

[54] J.A. Horsley and W.H. Fink, J. Chem. Phys. 50 (1969) 750.

[55] A.P. Hitchcock and C.E. Brion, J. Phys. B14 (1981) 4399.

[56] C.E. Brion, S.T. Hood, I.H. Suzuki, E. Weigold and G.R.S. Williams, J. Electron Spectry. 21 (1980) 71; C.E. Brion, I.E. McCarthy, I.H. Suzuki and E. Weigold, Chem. Phys. Letters 67 (1979) 115.

[57] M.S. Banna and D.A. Shirley, Chem. Phys. Letters 33 (1975) 441.

[58] W. von Niessen, L.S. Cedarbaum, W. Domcke and G.H.F. Diercksen, Chem. Phys. 56 (1981) 43.

[59] W.E. Moddeman, T.A. Carlson, M.O. Krause, B.P. Pullen, W.E. Bull and G.K. Schweitzer, J. Chem. Phys. 55 (1971) 2317.

[60] H. Agren, S. Svensson and V.I. Wahlgren, Chem. Phys. Letters 35 (1975) 336.

[61] H. Siegbahn, L. Asplund and P. Kelfre, Chem. Phys. Letters 35 (1975) 330.

[62] I.H. Hillier and J. Kendrick, Mol. Phys. 31 (1976) 849.

[63] H. Agren, J. Chem. Phys. 75 (1981) 1267; H. Agren and H. Siegbahn, Chem. Phys. Letters 69 (1980) 424; J. Müller, H. Agren, and O. Goscinski, Chem. Phys. Letters 38 (1979) 349.

[64] R.R. Rye, T.E. Madey, J.E. Houston and P.H. Holloway, J. Chem. Phys. 69 (1978) 1504; R.R. Rye, J.E. Houston, D.R. Jennison, T.E. Madey and P.H. Holloway, Ind. Eng. Chem. Prod. Res. Dev. 18 (1979) 2.

[65] D.E. Ramaker, Phys. Rev. B21 (1980) 4608.

[66] G.E. Laramore, to be published.

[67] N. Kosugi, T. Ohta and H. Kuroda, Chem. Phys. 50 (1980) 373.

[68] D.R. Jennison, J.A. Kelber and R.R. Rye, Phys. Rev. B15 (1982) 1384.

[69] U. Wahlgren, Mol. Phys. 33 (1977) 1109.

[70] S. Svensson, H. Agren and U.I. Wahlgren, Chem. Phys. Letters 38 (1976) 1.

[71] L.S. Cederbaum, W. Domcke and J. Schirmer, Phys. Rev. A22 (1980) 206.

[72] D.K. Creber, J.S. Tse and G.M. Bancroft, J. Chem. Phys. 72 (1980) 4291.

[73] R. Jaeger, J. Stohr, R. Treichler and K. Baberscke, Phys. Rev. Letters 47 (1981) 1300;

R. Jaeger, R. Treichler, and J. Stohr, Surface Sci. 117 (1982) 533.

[74] V.H. Dibeler, J.A. Walker and H.M. Rosenstock, J. Res. NBS 70A (1966) 459.

[75] C.I.M. Beenakker, F.J. de Heer, H.B. Krop, and G.R. Möhlmann, Chem. Phys. 6 (1974) 445.

[76] J. Appell and J. Durup, Intern. J. Mass Spectry. Ion. Phys. 10 (1972/3) 247.

[77] T.R. Govers, M. Gerard and R. Marx, Chem. Phys. 15 (1976) 185.

[78] H.H. Harris and J.J. Leventhal, J. Chem. Phys. 64 (1976) 3185.

[79] F. Fiquet-Fayard and P.M. Guyon, Mol. Phys. 2 (1966) 17.

[80] A.J. Lorquet and J.C. Lorquet, Chem. Phys. 4 (1974) 353.

[81] J.H.D. Eland, Chem. Phys. 11 (1975) 41.

[82] C.R. Brundle and D.W. Turner, Proc. Roy. Soc. A307 (1968) 27.

[83] R.H. Prince and G.R. Floyd, Chem. Phys. Letters 43 (1976) 326.

[84] T.E. Madey and J.T. Yates, Surface Sci. 63 (1977) 203.

[85] H.P.D. Liu and G. Verhaegen, Intern. J. Quantum Chem. 5 (1971) 103.

[86] J.A. Smith, P. Jorgensen and Y. Ohrn, J. Chem. Phys. 62 (1975) 1285.

[87] H. Sakai, S. Yamabe, T. Yamabe, K. Fukui and H. Kato, Chem. Phys. Letters 25 (1974) 541.

[88] P.J. Fortune, B.J. Rosenberg and A.C. Wahl, J. Chem. Phys. 65 (1976) 2201.

[89] R.A. Rouse, J. Chem. 64 (1976) 1244.

[90] G.B. Balint-Kurti and R.N. Yardley, Chem. Phys. Letters 36 (1975) 342.

[91] W.A. Goddard and W.J. Hunt, Chem. Letters 24 (1974) 464.

[92] C.R. Claydon, G.A. Segal and H.S. Taylor, J. Chem. Phys. 54 (1971) 3799.

[93] I. Easson and M.H.L. Pryce, Can. J. Phys. 51 (1973) 518.

[94] H.H. Michels and F.E. Harris, Chem. Phys. Letters 3 (1969) 441.

[95] A. Karo, M. Krauss and A.C. Wahl, Intern. J. Quantum Chem. 7# (1973) 143.

[96] W. Meyer, Theoret. Chim. Acta 35 (1974) 277.

[97] D.M. Hanson, R. Stockbauer and T.E. Madey, Phys. Rev. B24 (1981) 5513.

[98] S.L. Weng and O.F. Kammerer, Phys. Rev. B26 (1982) 2281.

[99] M.L. Knotek and J.E. Houston, J. Vac. Sci. Technol. 20 (1982) 544; to be published.

[100] S. Polezo and P. Fantucci, Gazz. Chim. Ital. 110 (1980) 557.

[101] C.F. Melius, R.H. Stulen and J.O. Noell, Phys. Rev. Letters 48 (1982); private communication.

[102] C.E. Brion, J.P.D. Cook and K.H. Tan, Chem. Phys. Letters 59 (1978) 241; J.P.D. Cook, C.E. Brion and A. Hamnett, J. Electron. Spectry. 15 (1979) 233; Chem. Phys. 45 (1980) 1.

TECHNICAL REPORT DISTRIBUTION LIST, GEN

	No. Copies		No. Copies
Office of Naval Research Attn: Code 413 800 North Quincy Street Arlington, Virginia 22217	2	Naval Ocean Systems Center Attn: Mr. Joe McCartney San Diego, California 92152	1
ONR Pasadena Detachment Attn: Dr. R. J. Marcus 1030 East Green Street Pasadena, California 91106	1	Naval Weapons Center Attn: Dr. A. B. Amster, Chemistry Division China Lake, California 93555	1
Commander, Naval Air Systems Command Attn: Code 310C (H. Rosenwasser) Department of the Navy Washington, D.C. 20360	1	Naval Civil Engineering Laboratory Attn: Dr. R. W. Drisko Port Hueneme, California 93401	1
Defense Technical Information Center Building 5, Cameron Station Alexandria, Virginia 22314	12	Dean William Tolles Naval Postgraduate School Monterey, California 93940	1
Dr. Fred Saalfeld Chemistry Division, Code 6100 Naval Research Laboratory Washington, D.C. 20375	1	Scientific Advisor Commandant of the Marine Corps (Code RD-1) Washington, D.C. 20380	1
U.S. Army Research Office Attn: CRD-AA-IP P. O. Box 12211 Research Triangle Park, N.C. 27709	1	Naval Ship Research and Development Center Attn: Dr. G. Bosmajian, Applied Chemistry Division Annapolis, Maryland 21401	1
Mr. Vincent Schaper DTNSRDC Code 2803 Annapolis, Maryland 21402	1	Mr. John Boyle Materials Branch Naval Ship Engineering Center Philadelphia, Pennsylvania 19112	1
Naval Ocean Systems Center Attn: Dr. S. Yamamoto Marine Sciences Division San Diego, California 91232	1	Mr. A. M. Anzalone Administrative Librarian PLASTEC/ARRADCOM Bldg 3401 Dover, New Jersey 07801	1

TECHNICAL REPORT DISTRIBUTION LIST, 056

	No. Copies		No. Copies
Dr. G. A. Somorjai Department of Chemistry University of California Berkeley, California 94720	1	Dr. W. Kohn Department of Physics University of California (San Diego) La Jolla, California 92037	1
Dr. J. Murday Naval Research Laboratory Surface Chemistry Division (6170) 455 Overlook Avenue, S.W. Washington, D.C. 20375	1	Dr. R. L. Park Director, Center of Materials Research University of Maryland College Park, Maryland 20742	1
Dr. J. B. Hudson Materials Division Rensselaer Polytechnic Institute Troy, New York 12181	1	Dr. W. T. Peria Electrical Engineering Department University of Minnesota Minneapolis, Minnesota 55455	1
Dr. Theodore E. Madey Surface Chemistry Section Department of Commerce National Bureau of Standards Washington, D.C. 20234	1	Dr. Chia-wei Woo Department of Physics Northwestern University Evanston, Illinois 60201	1
Dr. J. M. White Department of Chemistry University of Texas Austin, Texas 78712	1	Dr. Robert M. Hexter Department of Chemistry University of Minnesota Minneapolis, Minnesota 55455	1
Dr. Keith H. Johnson Department of Metallurgy and Materials Science Massachusetts Institute of Technology Cambridge, Massachusetts 02139	1	Dr. R. P. Van Duyne Chemistry Department Northwestern University Evanston, Illinois 60201	1
Dr. J. E. Demuth IBM Corporation Thomas J. Watson Research Center P. O. Box 218 Yorktown Heights, New York 10598	1	Dr. S. Sibener Department of Chemistry James Franck Institute 5640 Ellis Avenue Chicago, Illinois 60637	1
Dr. C. P. Flynn Department of Physics University of Illinois Urbana, Illinois 61801	1	Dr. M. G. Lagally Department of Metallurgical and Mining Engineering University of Wisconsin Madison, Wisconsin 53706	1

TECHNICAL REPORT DISTRIBUTION LIST, 056

No.   No.
Copies   Copies

Dr. John T. Yates
Department of Chemistry
University of Pittsburgh
Pittsburgh, Pennsylvania   15260

Professor G. H. Morrison
Department of Chemistry
Cornell University
Ithaca, New York   14853

Captain Lee Myers
AFOSR/NC
Bolling AFB
Washington, D.C.   20332

Dr. David Squire
Army Research Office
P. O. Box 12211
Research Triangle Park, NC   27709

Professor Ronald Hoffman
Department of Chemistry
Cornell University
Ithaca, New York   14853

TECHNICAL REPORT DISTRIBUTION LIST, 056

	No. Copies		No. Copies
Dr. Robert Gomer Department of Chemistry James Franck Institute 5640 Ellis Avenue Chicago, Illinois 60637	1	Dr. K. G. Spears Chemistry Department Northwestern University Evanston, Illinois 60201	1
Dr. R. G. Wallis Department of Physics University of California, Irvine Irvine, California 92664	1	Dr. R. W. Plummer University of Pennsylvania Department of Physics Philadelphia, Pennsylvania 19104	1
Dr. D. Ramaker Chemistry Department George Washington University Washington, D.C. 20052	1	Dr. E. Yeager Department of Chemistry Case Western Reserve University Cleveland, Ohio 41106	1
Dr. P. Hansma Physics Department University of California, Santa Barbara Santa Barbara, California 93106	1	Professor D. Hercules University of Pittsburgh Chemistry Department Pittsburgh, Pennsylvania 15260	1
Dr. J. C. Hemminger Chemistry Department University of California, Irvine Irvine, California 92717	1	Professor N. Winograd The Pennsylvania State University Department of Chemistry University Park, Pennsylvania 16802	1
Dr. Martin Fleischmann Department of Chemistry Southampton University Southampton SO9 5NH Hampshire, England	1	Professor T. F. George The University of Rochester Chemistry Department Rochester, New York 14627	
Dr. G. Rubloff IBM Thomas J. Watson Research Center P. O. Box 218 Yorktown Heights, New York 10598	1	Professor Dudley R. Herschbach Harvard College Office for Research Contracts 1350 Massachusetts Avenue Cambridge, Massachusetts 02138	1
Dr. J. A. Gardner Department of Physics Oregon State University Corvallis, Oregon 97331	1	Professor Horia Metiu University of California, Santa Barbara Chemistry Department Santa Barbara, California 93106	
Dr. G. D. Stein Mechanical Engineering Department Northwestern University Evanston, Illinois 60201	1	Professor A. Steckl Rensselaer Polytechnic Institute Department of Electrical and Systems Engineering Integrated Circuits Laboratories Troy, New York 12181	

END

FILMED

12-83

DTIC